



3D numerical reconstruction of well-connected porous structure of rock using fractal algorithms

Yang Ju^{a,b,*}, Jiangtao Zheng^a, Marcelo Epstein^c, Les Sudak^c, Jinbo Wang^a, Xi Zhao^a

^a State Key Laboratory of Coal Resources and Safe Mining, China University of Mining & Technology (Beijing), Beijing 100083, China

^b State Key Laboratory for Geomechanics and Deep Underground Engineering, China University of Mining & Technology, Xuzhou 221116, China

^c Department of Mechanical and Manufacturing Engineering, University of Calgary, 2500 University Drive NW, AB T2N 1N4, Canada

Received 15 April 2013; received in revised form 13 June 2014; accepted 24 June 2014

Available online 1 July 2014

Abstract

Natural rock, such as sandstone, has a large number of discontinuous, multi-scale, geometry-irregular pores, forming a complex porous structure. This porous structure essentially determines the rock's physical and/or mechanical properties, which are of great significance to a variety of applications in the fields of science and engineering. As a supplement to experimental observation, a reliable reconstruction model of porous structure could provide an effective and economical way to characterize the physical and mechanical properties of a porous rock. In this paper, we present a novel method for reconstructing the well-connected porous structure of sandstones, which are often intractable to handle for current reconstruction methods. A fractal descriptor is here proposed for better characterizing complex pore morphologies. The reconstruction procedure of a 3D well-connected porous structure is optimized by integrating the improved simulated annealing algorithm and the fractal system control function. The proposed reconstruction method enables us to represent a large-size 3D porous structure. To verify the accuracy of reconstruction, we have analyzed the geometrical, topological, and mechanical properties of the reconstructed porous medium and compared them with those of prototype rock samples. The comparisons show good agreement between the reconstructed model and the real porous sandstone.

© 2014 Elsevier B.V. All rights reserved.

Keywords: Three-dimensional reconstruction; Porous structure; Sandstone; Fractal system control function; Simulated annealing; Mechanical properties

1. Introduction

Porous sandstone is a typical sedimentary rock encountered in many practical engineering applications, such as petroleum exploitation, underground mining, hydrogeology, CO₂ geological sequestration, and contaminant cleanup. It naturally involves a large number of discontinuous, multi-scale and geometrically irregular pores [1,2]. Essentially,

* Corresponding author at: State Key Laboratory of Coal Resources and Safe Mining, China University of Mining & Technology (Beijing), Beijing 100083, China. Tel.: +86 10 62331490.

E-mail addresses: yju@me.com, juy@cumtb.edu.cn (Y. Ju).

the macroscopic physical and mechanical properties of sandstone are determined by its porous microstructure. For example, the inherent topological network structure of pores greatly affects the flow behavior of fluids in rock [3–5], while the oil and gas production capacity of reservoir rocks is primarily dominated by its porosity and permeability [6]. Specially, the rock permeability, which is crucial for CO₂ sequestration and nuclear waste disposal, is predominantly determined by pore connectivity [7]. In addition, the microstructure of pores also exerts great influence on rock mechanical properties such as elastic modulus, Poisson's ratio, strength, and failure mechanisms [8–11]. Accurate knowledge and characterization of the nature of pore systems, including the geometry, population, distribution and interrelationships, are of great significance in determining the physical and/or mechanical properties of sandstone [10,11]. However, this problem has not yet been settled satisfactorily due to the difficulties and challenges involved in experimental techniques and analytical theories.

In practice, macroscopic properties are usually specified by corresponding experiments on rock core samples. However, as human activities such as energy resource exploitation extend to areas of complex geology, rock sample drilling could cost millions of dollars. The experiments conducted on limited amount of core samples are incapable of uncovering the intrinsic mechanisms that lead to the different measurement results in different rock samples. Repeated drilling at different sites and more experimental analyses are required in order to get accurate rock property specifications. This dilemma not only increases engineering costs, but also raises discrepancies in the description of the microstructure and mechanical properties of rock between the different samples, due to the inhomogeneity, heterogeneity and discontinuity of sandstones. On the other hand, the internal mechanisms, such as multi-phase fluid flow behavior inside the rock, and pore structure evolution while the rock sample is under applied forces, cannot be determined through these tests. This situation motivates researchers to consider an alternative approach, using as few core samples as possible to characterize the microstructure and the corresponding physical and/or mechanical properties of porous rock.

Besides the experimental specification of rock properties, researchers have proposed a few theoretical models, such as continuum models, double or dual porosity models, to mention just a few, to specify the rock mechanical behavior accounting for pore influences. These theoretical models, however, have been established solely to determine some specific properties of porous media [12–19]. Part of what causes the difficulty for the analytical models to take account of the nature of porous structure, from the mathematical perspective, is that the pore structure is too complicated to have a precise analytical description. Pores randomly distribute, ranging several orders of magnitudes in size, leading to the difficulty in achieving a close description of these features. In addition, a pore or cavity is geometrically irregular, i.e., has a rough boundary, which makes it extremely intractable to model either in mathematics or in physics. As a result, predicting porous-rock mechanical properties using an analytical model becomes either incorrect or greatly different from the experimental results. This raises the question as to whether there is a proper way to get an explicit description of the complex microstructure, based on which the macroscopic or external physical and/or mechanical properties could be predicted.

It is clear that the accurate knowledge of the pore microstructure system is of essential significance for disclosing the intrinsic mechanisms that govern the mechanics of rock, and for linking those mechanisms with the apparent mechanical behavior. It requires a reliable quantitative characterization of pore structure through which the external macroscopic properties of rock can be determined. Neither phenomenological core tests nor theoretical models can satisfy this requirement. Several advanced experimental methods have been used to measure the porous microstructure of rock. Two-dimensional (2D) thin section images of rock pore networks can be obtained using scanning electron microscope (SEM) [20] or focused ion beam (FIB) system [21]. Three-dimensional (3D) images of pore structure can be obtained by using a non-destructive X-ray computed micro-tomography (CT) [22]. Although CT images have a relatively lower spatial resolution than SEM or FIB, it provides a direct 3D description of the porous structure, and therefore offers the information necessary for studying macroscopic rock properties, such as elastic modulus, Poisson's ratio, porosity, permeability, and their correlation to the microstructure.

However, attaining an accurate description of the 3D microstructure of porous rock is difficult, laborious, time consuming, and economically expensive with the use of advanced 3D CT measurement techniques, e.g. synchrotron X-ray computed microtomography [23,24]. This raises the question of whether there is a method to attain a reliable 3D model properly representing the microstructure of porous rock by conducting as few CT tests as possible. Digital rock-model-reconstruction methods using limited structural information could provide an effective and economical way to achieve the purpose. Several methods for reconstructing a 3D porous structure have been developed, such as statistical-information-based method [25–27], process-based method [28], pore-network method [29], continuum

reconstruction method [30]. Among them, the process-based method, which builds the 3D pore structure by imitating the rock formation process (especially sedimentary rocks) based on the petrographical information extracted from an actual rock, is particularly promising. This method is very attractive for reconstructing 3D pore network of the sandstones with clear granular matrices. However, it may not be able to handle rocks which experienced more complex geological history such as significant compaction, dissolution, and chemical reaction [31]. Another method is statistical-information-based reconstruction, in which the reconstructed model is continuously adjusted to match the statistical properties measured from the CT images or SEM scan images of actual rock samples. The statistical reconstruction can be achieved by several methods; among them, the simulated annealing algorithm (SAA) reconstruction is particularly attractive. It is capable of reconstructing the 3D microstructure of any type of rocks. Particularly, it can contain as much statistical information as possible, limited only by computer calculation capacity. Having said that, it is also true that the SAA reconstruction method possesses several limitations as well. First of all, it is usually very hard to represent the well-connected pore networks for its complex pore morphology. Second, the computation time increases exponentially with model size, which makes it incapable of reconstructing a large-size 3D microstructure. But the porous structure of natural rock is heterogeneous, which means the representative model must have an adequate size, based on which the basic properties of rock can be accurately studied. The size of most current reconstruction models cannot meet this requirement. Finally, most of the current reconstruction models focus on the mathematical similarity with the real rock structures, rather than on whether the models could be used to analyze and predict the physical and/or mechanical properties of rock.

We aim at developing a faster, more accurate, and more efficient optimization algorithm for creating a 3D model of porous-rock microstructure, based on which the prediction and analysis of the physical and/or mechanical behavior of porous rock can be performed. To achieve this goal, we introduce an improved SAA reconstruction method. The proposed method can be used to reconstruct large-size, well-connected porous structure efficiently. Specifically, a so-called multiple interchanging algorithm has been incorporated into the program to improve the preliminary reconstruction model. Moreover, a fractal descriptor characterizing complex pore morphologies is introduced in the reconstruction process. Furthermore, a novel system updating algorithm, called pre-conditioning algorithm, is proposed to enhance the reconstruction efficiency in the later stage, by which the reconstruction process could converge more quickly. It is worth noting that, contrary to most previous 3D reconstruction methods, which are based on the information extracted from 2D thin section images [28,32], the proposed method directly reconstructs the 3D microstructure from a 3D image generated from a series of 2D thin section CT images.

For the purpose of evaluating the effectiveness of the reconstruction model, we compare the reconstructed model with the real rock model in terms of statistical information, pore geometric distribution, topological parameters, and mechanical properties. Compared with previous methods, the proposed 3D microstructure reconstruction method reproduces more accurately the intrinsic characteristics of the actual sandstone. In addition, the proposed method exhibits higher reconstruction efficiency.

The remainder of the paper is structured as follows: in Section 2 for the sake of clarity the proposed method is presented through a 2D porous rock model reconstruction, with emphasis on the several improvements to conventional SAA. In Section 3, we employ the proposed method to reconstruct a 3D microstructure based on the information extracted from CT images of an actual rock sample. In Section 4, the reconstructed microstructure is compared with that of the actual rock model in terms of topological parameters and mechanical properties. We make concluding remarks in Section 5.

2. Methodology

2.1. General procedure

The proposed reconstruction method is based on the framework of a conventional SAA. First, a binary image (Fig. 1) containing only black (pores) and white (solid matrix) points (or pixels) is obtained through image processing [33–35] of original CT images of an actual sandstone sample. We chose Otsu's segmentation method [33], i.e., a global thresholding and optimization algorithm, to process the original CT images. As pointed out in [35], while local segmentation methods [36,37] can generally provide better segmentation quality and account for some image artifacts (e.g., beam hardening, or high-frequency noise), but they make much greater computational and memory demands. In this study, we are concerned more about pursuing a proper image processing algorithm that

is capable of quickly processing many images of complex pore structures with rough boundaries, enabling a rapid 3D representation with low computation demand. At the same time, we expect that the processing algorithm can provide better binarization results including having consistent porosity with the experimentally measured value of rock compared to the other tested global thresholding methods [38,39]. Based on these considerations, we employed the Otsu's segmentation method for the CT image processing and optimization. Using a binary image not only simplifies the reconstruction process, but also highlights the characteristics of microstructures. This binary image of the actual sandstone was regarded as the reference model in the reconstruction process. Second, a randomly distributed black-and-white point structure was constructed and served as the initial reconstruction model, in which the total numbers of the black and white grid points (pixels) were set exactly the same as in the reference model. Then, the statistical information was extracted from both the reference model and the reconstruction model, and quantified in terms of control function values. The values of control functions from the reference model served as the target that the reconstruction model is required to match. The reconstruction was carried out by first making a trial position interchange between a pair of black and white grid points followed by determining whether to accept or reject the interchange. Let $f_0(r_i)$ represent the control function values of the reference model, and let $f(r_i)$ and $f'(r_i)$ represent the control function values of the reconstruction model before and after position interchange, respectively. The control function differences between the two reconstruction models and the reference model, which we call "Energy", was defined by Eqs. (1) and (2), respectively:

$$E = \sum_i [f(r_i) - f_0(r_i)]^2 \quad (1)$$

$$E' = \sum_i [f'(r_i) - f_0(r_i)]^2 \quad (2)$$

$$\Delta E = E' - E \quad (3)$$

where E and E' are the "Energy" of the reconstruction model before and after the pixel-position interchange. The position interchange is accepted with probability $p(\Delta E)$ according to the Metropolis criterion [25]:

$$p(\Delta E) = \begin{cases} 1 & \Delta E \leq 0 \\ \exp(-\Delta E/T) & \Delta E > 0 \end{cases} \quad (4)$$

where T decreases slowly over time and should be set relatively high at the beginning.

2.2. Multiple interchanging process

The formation of various sized white blocks by the aggregation of randomly distributed white grid points is observed in traditional SAA during the preliminary reconstruction stage of well-connected porous sandstone. However, the formation of these white blocks requires a slowly decreasing rate of T , which makes the reconstruction time-consuming. To solve this problem, a multiple interchanging process (MIP) is proposed in this work to accelerate the formation of preliminary white blocks. In MIP, instead of interchanging a pair of black and white grid points, multiple black grid points within a block are exchanged simultaneously with the white points randomly picked from the entire image area. The "Energy" difference is subsequently calculated to determine whether to accept or reject the MIP move. A white block formed after the black points within the region are all exchanged by the white grid points. The target size and number of white blocks are set according to statistical information extracted from the reference model. A 2D preliminary reconstruction structure built via MIP was shown in Fig. 2.

2.3. Fractal system control function

It has been shown by numerous studies [40–42] that the microstructures of rock can be well described using fractal geometry. In this work, a fractal dimension measurement was introduced into the code to provide a better characterization of complex pore morphologies. A variety of fractal dimension measurements can be found in the literature [42–44]. In this paper, a fractal descriptor based on the box-covering [45] fractal measurement was employed to set up the fractal system control function. Specifically, the image was covered by small squares of a certain size, and then the probability that the pixels within a small square are all white is calculated, as shown in Fig. 3. For simplicity of

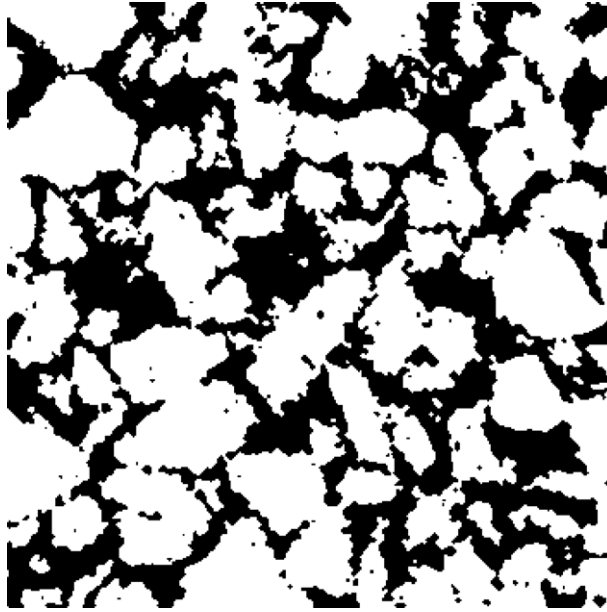


Fig. 1. The 2D binary reference model with a size of 352×352 pixels.

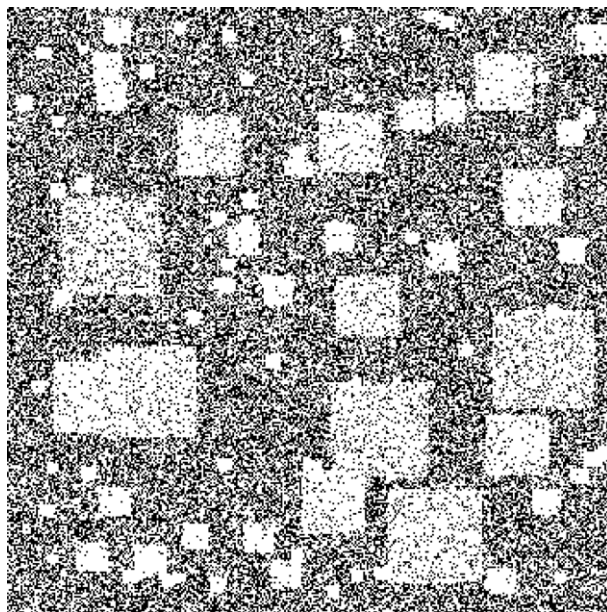


Fig. 2. 2D preliminary reconstruction structure built via MIP.

the reconstruction program, the fractal system control function is determined only in the three orthogonal directions. The fractal system control function in XY slice is defined as follows:

$$\begin{aligned}
 F^j(r) = & \langle I^j(x, y, z)I^j(x + 1, y, z) \dots I^j(x + r, y, z) \\
 & I^j(x, y + 1, z)I^j(x + 1, y + 1, z) \dots I^j(x + r, y + 1, z) \\
 & \vdots \\
 & I^j(x, y + r, z)I^j(x + 1, y + r, z) \dots I^j(x + r, y + r, z) \rangle
 \end{aligned} \tag{5}$$

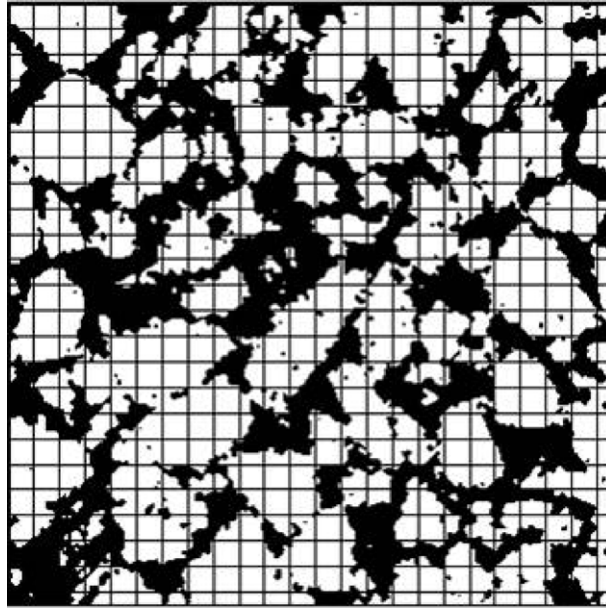


Fig. 3. Determination of the fractal descriptor and the fractal system control function using box-covering method.

where r is the side length of small squares; j denotes the statistical phase, with the solid phase chosen in the fractal system control function; $I^j(\mathbf{r}_i)$ is the characteristic function defined by [25]:

$$I^j(\mathbf{r}_i) = \begin{cases} 1, & \text{when } \mathbf{r}_i \text{ is in phase } j \\ 0, & \text{others.} \end{cases} \quad (6)$$

The multiplication result of all the $I^j(\mathbf{r}_i)$ in the angular brackets represents whether or not all the points are white in one box with side r . The angular brackets indicate the ensemble average of the multiplication result over the whole three dimension model. In other words, the value of $F^j(r)$ represents the percentage of the covering-boxes with side r completely filled by white points. The side length of a box, r , for determining $F^j(r)$ ranges within 2 to 36 pixels.

Other control functions employed in the proposed reconstruction method include the classic two-point probability control function and the linear-path control function, which are described in detail in papers by Yeong and Torquato [25,46]. The two-point probability control function contains the distribution information of black and white points, while the linear-path control function and fractal system control function contain the connectedness information for pores or solid phase. They are combined together with their own weightiness factor in the reconstruction procedure, which ensures that their initial “Energy” values are similar.

2.4. Pre-conditioning procedure

One of the inherent characteristics of the conventional SAA algorithm is that the percentage of accepted position interchanges decreases drastically with iteration steps, as shown in Fig. 4. As the control function value of reconstructed microstructure approaches closer to that of the reference model, the energy difference ΔE is more likely positive, due to the random selection of interchanging grid points. Moreover, the probability of acceptance becomes even smaller as T decreases. Consequently, only a very small proportion of position interchanges are accepted, and the evolution of the reconstructed structure becomes very slow. Meanwhile, the control function value does not change when the position interchange is rejected. As a result, most of the time spent in updating control functions is ineffective. Furthermore, we observed that most grid points undergoing successful position interchange were most likely isolated, as shown in Fig. 5(a) and (b), which corresponds to Step 8 and Step 10 in Fig. 4.

In this work, a pre-conditioning procedure was developed. It was carried out before determining the control functions. In a typical pre-conditioning procedure, a pair of isolated black and white points were selected instead of random choosing. The control functions were subsequently calculated to determine whether to accept this position

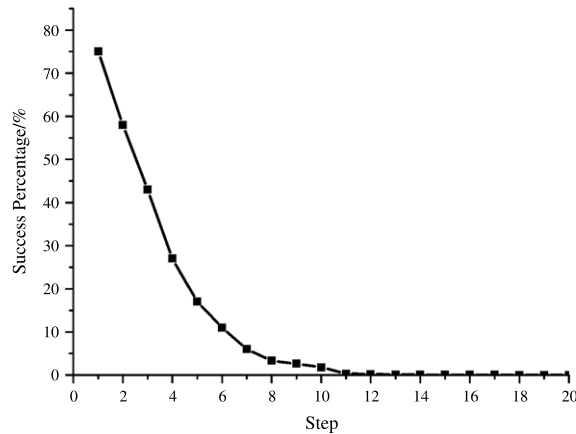


Fig. 4. Acceptant percentage of position interchange in conventional SAA.

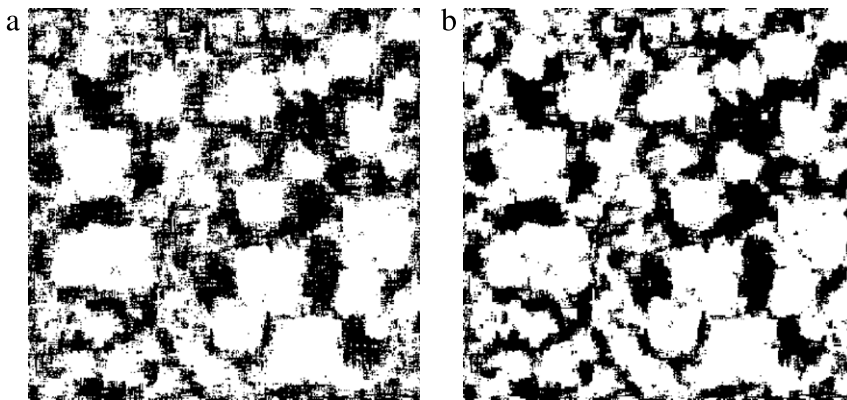


Fig. 5. Intermediate reconstructed structures. (a) When 200 consecutive unsuccessful interchanges first appeared. (b) When 500 consecutive unsuccessful interchanges first appeared.

interchange. In this way, the pre-conditioning enhanced the acceptance percentage and greatly reduced much of the unnecessary determination time of control functions in the later stage of reconstruction. It should be emphasized that the pre-conditioning procedure was performed only after the basic porous reconstruction structure had been established. The procedure accelerated the reconstruction without breaking the acceptance criteria by choosing a pair of grid points that were more likely to be successfully interchanged. In fact, the acceptance of an interchange was still determined by the Metropolis law. Fig. 6 shows the reconstructed structures before and after performing the pre-conditioning procedure.

For a better understanding of the entire reconstruction process, several representative structures from a 2D porous rock reconstruction are given in Fig. 7.

3. 3D microstructure reconstruction

The proposed method was successfully utilized to reconstruct a 3D image ($70 \times 352 \times 352$) of well-connected porous structures based on the statistical information from the 3D CT images. First, we built an arbitrary 3D structure possessing the same porosity as that of the reference model. The porosity was kept the same throughout the reconstruction, because the total number of white and black voxels was constant. Then, several hexahedron-shaped solids were cast in the reconstructed model via MIP, based on the morphological information from the reference model. The two-point probability control function was employed in this specific step, because it provided the spatial distribution information for pores and solid matrix. After the preliminary structure was built, the conventional SAA was subsequently employed and the two-point probability control function, linear-path control function and

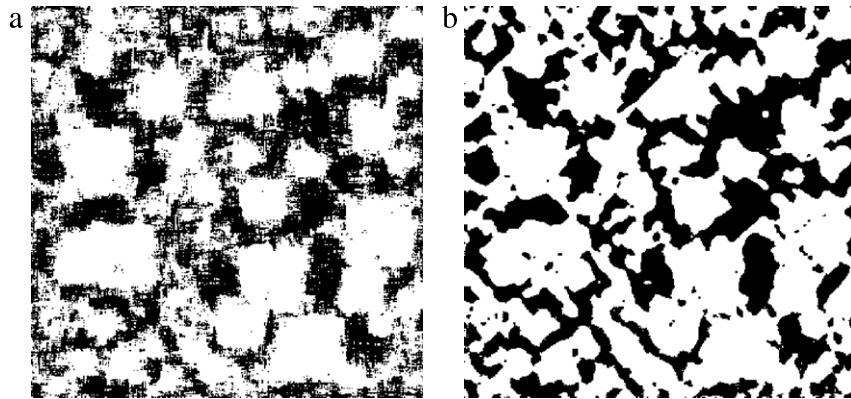


Fig. 6. Intermediate reconstructed structures. (a) Before performing the pre-conditioning procedure. (b) After performing the pre-conditioning procedure.

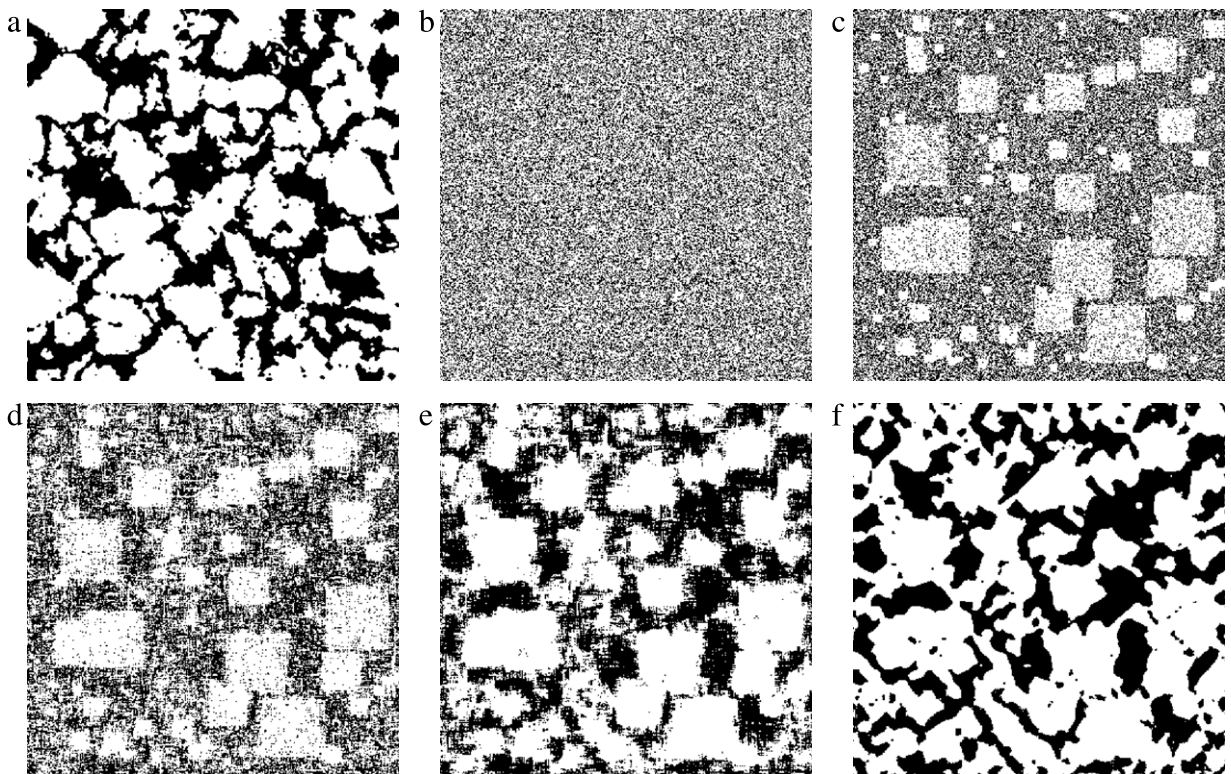


Fig. 7. Representative structures obtained in a 2D reconstruction of well-connected porous rock. (a) Reference model. (b) Randomly distributed points model. (c) Preliminary model generated by MIP. (d) After 50 consecutively unsuccessful interchanges model. (e) After 200 consecutively unsuccessful interchanges model. (f) Final reconstruction model after carrying out the pre-conditioning procedure.

fractal system control function were adopted. If 200 position interchanges consecutively rejected by the program, the pre-conditioning procedure was introduced and performed before determining the control functions. After these steps, the reconstructed 3D microstructure will possess almost the same control function values as those of the reference model, shown in Fig. 8. The reconstructed 3D microstructure and the reference model were visualized using MIMICS[®] (<http://biomedical.materialise.com/mimics>) for comparing the geometric configuration of porous structure (see Fig. 9). As shown in Fig. 9, both models demonstrate fairly similar 3D microstructures, even though their surface pore morphologies appear different. The topological and mechanical properties of these two models will be compared in the next section.

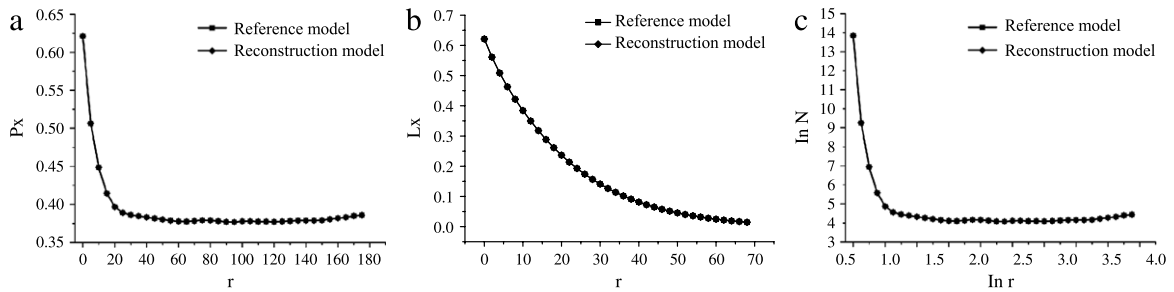


Fig. 8. Comparison of the control function values between the reference and reconstruction models. (a) Two-point control function. (b) Linear path control function. (c) Fractal system control function.

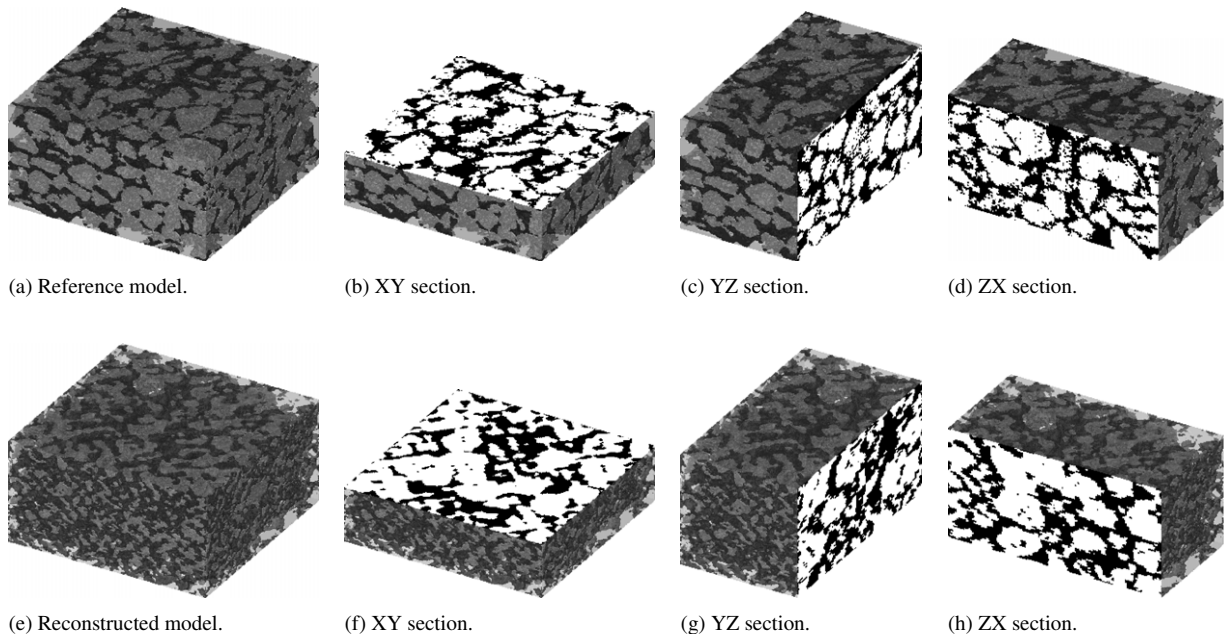


Fig. 9. 3D visualization of reference and reconstruction models.

4. Comparison of topological parameters and mechanical properties between reconstruction and reference models

The evaluation of the reconstructed microstructure is an important part of model reconstruction [47–49], in that it provides a quantitative description of the accuracy of the reconstruction. Most evaluation are focused on the statistical structural properties [47,48]. However, such an evaluation does not touch the topological, physical, and mechanical properties that are of most concern in engineering, such as pore-throat ratio, elasticity modulus, strength, and permeability. Rather than just concentrate on a comparison of geometric characteristics, we extend to compare topological and mechanical properties of the reconstruction and reference models.

4.1. Topological parameters

The topological parameters compared between reference and reconstruction model are the number of pores (relative large pores), number of throats (narrow pores that connect large pores) and the average coordination number of pores (average number of throats that a pore connects). We developed a so-called *Geometric and Topological Properties Analysis of Porous Rock Structure* code to identify the pores and throats of the pore space. In order to efficiently implement the algorithm, we first employed the watershed algorithm [50,51] to separate the pore space into isolated

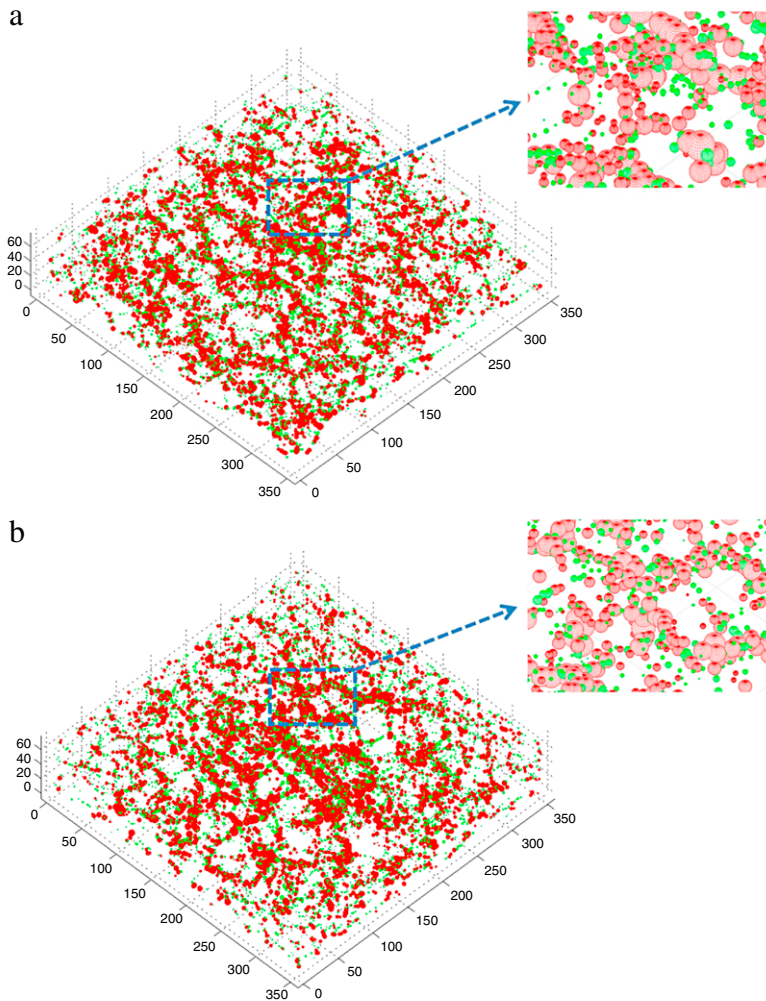


Fig. 10. Pore body (red sphere) and throat body distribution (green sphere). (a) Reference model. (b) Reconstruction model.

sectors. This method greatly enhances the efficiency of the following calculations. Then, the burning algorithm [52] was used to extract the skeleton of each individual sector rather than the whole pore structure. After that, the skeletons of neighbor pore space were connected with each other to form the entire skeleton of the pore space. During these processes, the burn number (or maximum inscribed sphere radius) of each skeleton voxel was recorded. The skeleton voxels that have local maximum and minimum burn number were chosen as the center of each pore space and throat space. Finally, the topologically equivalent structure was established, through which the topological parameters of the real and reconstructed porous structures were extracted. We wrote a computer program for the algorithms, which reads the image data and outputs the geometric and topological parameters of pore space automatically. Actually, the algorithm we employed to generate the equivalent network of pore space is, to some extent, similar to the “medial-axis based approach” reviewed by Al-Raoush, Thompson and Willson [53], except that we add the watershed algorithm at the beginning, which helps efficiently identify a complex porous structure into some relatively simple pore spaces. For more details of the “medial-axis based approach” and its revised version, please refer to the references [53–55]. The accuracy of the *Geometric and Topological Properties Analysis of Porous Rock Structure* code was verified using a regular packing sphere model. Table 1 lists the calculation results. It is shown that the values of the coordination number for both the reference model and the reconstruction model are very close. Fig. 10 compares the distribution of pore body and throat body for the reference model and the reconstruction model.

Table 1
Topological parameters of the reference model and the reconstructed model.

Model	Number of pores	Number of throats	Average coordination number of pores
Reference	3394	5675	4.082
Reconstructed	3161	5240	4.067

Table 2
Material parameters employed in FEM simulations.

Model	Elastic modulus (GPa)	Poisson's ratio	Internal friction angle (°)	Cohesive strength (MPa)	Plastic shear stiffness (GPa)	Residual strength (MPa)
Pore	4	0.2	15	2	−0.4	0.05
Matrix	40	0.3	20	20	−4	0.5

4.2. Physical and/or mechanical properties

The mechanical properties of both models were analyzed using the finite element method (FEM). MIMICS[®] (<http://biomedical.materialise.com/mimics>) was employed to convert the two graphic models into FEM meshed models. Regarding the creation of the FEM model, we adopted some built in algorithms in MIMICS to create, clean-up, and optimize finite element meshes from the voxelized representation of porous structure. As concerned, the morphology of microstructure appears to be irregular, which could cause thorny problems, such as the large number of elements with small size, mesh distortion, and complex interfaces, which are normally difficult to handle in numerical implementation. This requires a lot of mesh clean-up and optimization work. We took the following measures to solve these problems. In order to reduce the number of bad meshes and to generate high quality finite element meshes, we first applied the built-in algorithms “medfilt3” [56] and “bwareaopen” of MATLAB to the voxelized 3D entity to eliminate the isolated matrix voxels and pore voxels. These isolated voxels mainly refer to those points that distribute within the rock grains and pores. The fraction of these eliminated voxels is less than 1/1000 of total rock matrix voxels and total pore voxels, respectively. The optimized voxelized images were then imported into MIMICS to create a 3D entity using the built-in algorithms “Create Masks” and “Calculate 3D Models”. After that, by operating “Remeshing”, we initiated the triangle surface meshes using 3-matic (a sub-module in MIMICS) at the outer surface of the model. The tetrahedron volume meshes were then created from the surface meshes and extended to the interior of the entity, also using 3-matic operation. Each triangle must comply with the following rules to ensure the quality of meshes: (1) the maximum side length must be shorter than the length of 10 voxels, and (2) the minimum height/bottom side length ratio must be larger than 0.4. Finally, each tetrahedron element is attributed with either rock matrix or porous material properties, according to its position in the 3D entity.

The two meshed models were subsequently analyzed through finite element analysis program *SciFEA* developed by our own. The uniaxial compression tests were conducted numerically by using the 3D elastoplastic softening module in *SciFEA*. The Drucker–Prager criterion was set as the plastic yield criterion. After the stress exceeded the criterion, the stress of an element would be set to decrease rather than increase along with increasing strain, and finally down to the residual strength. For comparing the mechanical responses of the two models, we attributed relatively high mechanical parameter values to the matrix phase (in accordance with our previous experimental results) and low values to the pore phase. The pore phase was considered as the low-strength bonding material rather than the void space. Therefore, we did not set the material properties of pore phase to be null. We conceptually set the pore phase to be about one-tenth the mechanical parameter values of the matrix phase such as for elastic modulus, cohesive strength, and residual strength. Table 2 lists the material parameters employed in the simulations.

The displacement along the loading direction and the contour of first principal stress are illustrated in Fig. 11 and Fig. 12, respectively. As we can see in Fig. 12, the stress of rock matrix elements are generally higher than that of pore element. Still, the differences occurred on the surface. However, the integrated mechanical properties are similar in the two models. Fig. 13 plots the resulting stress–strain responses for both reconstruction and reference models. It is evident that the two response curves are very close to each other. Moreover, the elastic modulus, the Poisson's ratios and the compression strength in both models are considerably close, as shown in Table 3. These results indicate that the reconstructed microstructure could be safely utilized to predict rock mechanical properties.

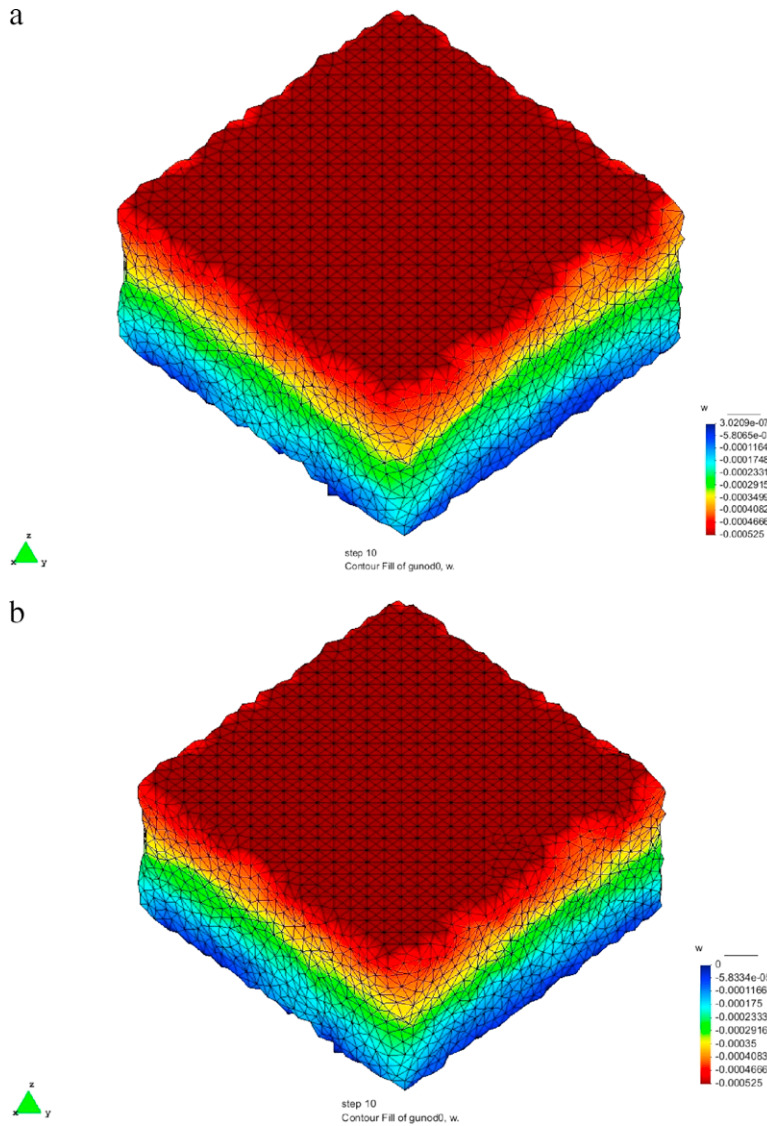


Fig. 11. Displacement in Z direction. (a) Reference model. (b) Reconstruction model.

Table 3
Mechanical properties of reference and reconstruction models.

Model	Elastic modulus (GPa)	Poisson's ratio	Compression strength (MPa)
Reference	23.582	0.214	18.735
Reconstructed	23.819	0.212	19.087

5. Conclusions

In this paper, a faster, more accurate, and more efficient reconstruction algorithm (compared to current reconstruction algorithms) has been developed for representing the 3D porous microstructure of well-connected sandstone. Specifically, a MIP procedure was incorporated to accelerate the evolution of the preliminary structure, which ensures better final reconstruction results. A fractal descriptor and a fractal system control function were introduced in the reconstruction procedure. The fractal system control function along with the two-point probability

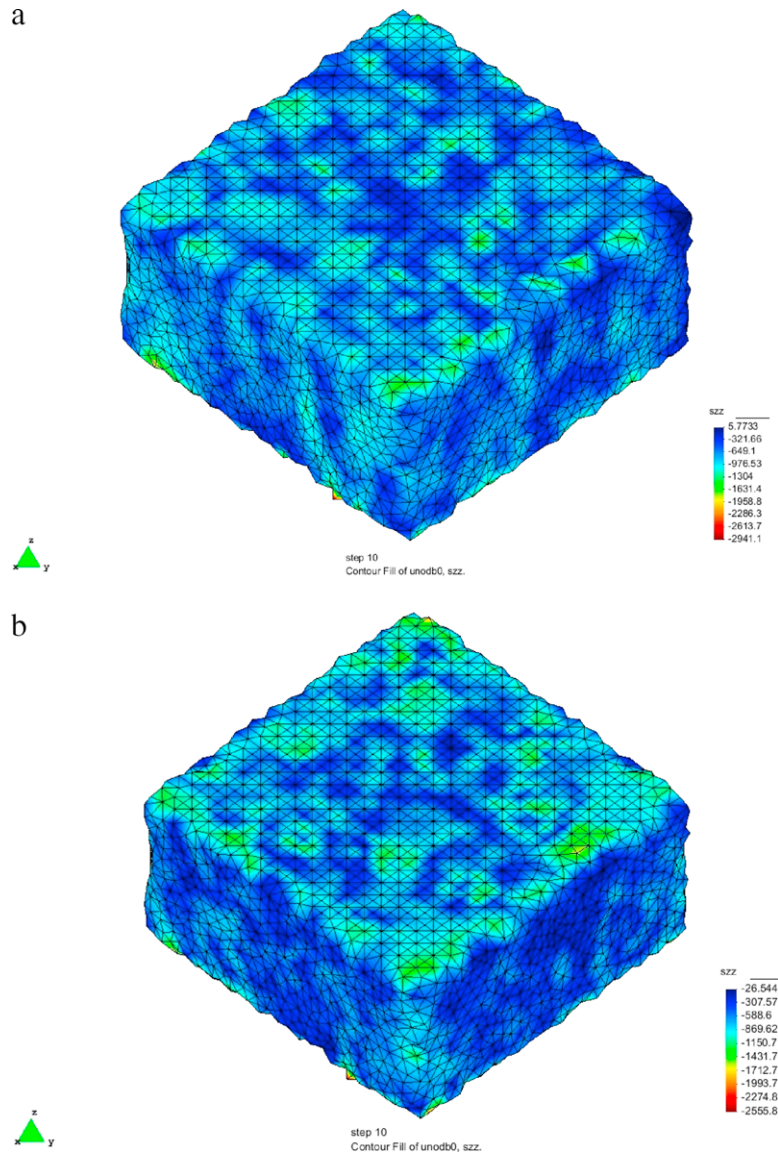


Fig. 12. First principal stress nephogram. (a) Reference model. (b) Reconstruction model.

control function and the linear-path control function can provide a better description of complex pore structures as well as ensure the effectiveness of reconstruction. Pre-conditioning procedure was carried out to speed up the convergence of reconstruction process. All of these improvements endow the proposed method with the capability of representing the microstructures of rocks with larger sizes and more complex porous structures compared to conventional methods such as the SAA algorithm.

The proposed method was applied in reconstructing a 3D well-connected porous microstructure based on a 3D reference model generated from CT images of an real sandstone. The comparison of the reconstructed model and the reference model shows good consistency between the three control functions.

The proposed method was also validated by comparing the topological parameters and the mechanical properties between the reconstruction model and the reference model. A computer algorithm and program was implemented to analyze the topological characters of pore space. A few tactics were adopted to optimize the reconstructed model and meshes, in order to facilitate FEM analysis of the medium's mechanical responses. The results show that both the topological and the mechanical properties of the two models are in good agreement.

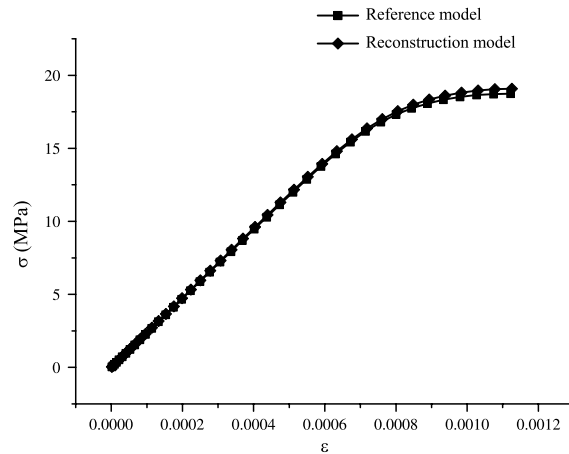


Fig. 13. Stress–strain responses of reference and reconstruction models.

Acknowledgments

We gratefully acknowledge the financial supports from the National Natural Science Foundation for Distinguished Young Scholars of China (Grant 51125017), the National Basic Research Program of China (Grant 2010CB226804, 2011CB201201), and the National Natural Science Foundation of China (Grant 51374213). The authors are grateful to the anonymous reviewers for their valuable comments and suggestions.

References

- [1] H. Xie, J.-A. Wang, M. Kwańniewski, Multifractal characterization of rock fracture surfaces, *Int. J. Rock Mech. Min.* 36 (1) (1999) 19–27.
- [2] A.J. Katz, A.H. Thompson, Fractal sandstone pores: implications for conductivity and pore formation, *Phys. Rev. Lett.* 54 (1985) 1325–1328.
- [3] M. Kainourgiakis, E. Kikkinides, A. Galani, G. Charalambopoulou, A. Stubos, Digitally reconstructed porous media: transport and sorption properties, *Transp. Porous Med.* 58 (1) (2005) 43–62.
- [4] B. Yu, M. Zou, Y. Feng, Permeability of fractal porous media by monte carlo simulations, *Int. J. Heat Mass Transfer* 48 (13) (2005) 2787–2794.
- [5] J. Cai, X. Huai, Study on fluid–solid coupling heat transfer in fractal porous medium by lattice Boltzmann method, *Appl. Therm. Eng.* 30 (6) (2010) 715–723.
- [6] A. Dixit, J. Buckley, S. McDougall, K. Sorbie, Empirical measures of wettability in porous media and the relationship between them derived from pore-scale modelling, *Transp. Porous Med.* 40 (1) (2000) 27–54.
- [7] D.C.M. White, B.R. Strazisar, E.J. Granite, J.S. Hoffman, H.W. Pennline, Separation and capture of CO₂ from large stationary sources and sequestration in geological formations coalbeds and deep saline aquifers, *J. Air Waste Manage.* 53 (6) (2003) 645–715.
- [8] H.H. Liu, J. Rutqvist, J.G. Berryman, On the relationship between stress and elastic strain for porous and fractured rock, *Int. J. Rock Mech. Min.* 46 (2) (2009) 289–296.
- [9] R.J. Brown, J. Korrinda, On the dependence of the elastic properties of a porous rock on the compressibility of the pore fluid, *Geophysics* 40 (4) (1975) 608–616.
- [10] Y. Ju, Y. Yang, Z. Song, W. Xu, A statistical model for porous structure of rocks, *Sci. China Ser. E* 51 (11) (2008) 2040–2058.
- [11] Y. Ju, H. Wang, Y. Yang, Q. Hu, R. Peng, Numerical simulation of mechanisms of deformation, failure and energy dissipation in porous rock media subjected to wave stresses, *Sci. China Ser. E* 53 (4) (2010) 1098–1113.
- [12] M. Biot, Variational lagrangian-thermodynamics of nonisothermal finite strain mechanics of porous solids and thermomolecular diffusion, *Int. J. Solids Struct.* 13 (6) (1977) 579–597.
- [13] M.A. Biot, Theory of propagation of elastic waves in a fluid-saturated porous solid. i. Low-frequency range, *J. Acoust. Soc. Am.* 28 (2) (1956) 168–178.
- [14] M.S. Diallo, E. Appel, Acoustic wave propagation in saturated porous media: reformulation of the biot/squirt flow theory, *J. Appl. Geophys.* 44 (4) (2000) 313–325.
- [15] M. Kimura, Velocity dispersion and attenuation in granular marine sediments: comparison of measurements with predictions using acoustic models, *J. Acoust. Soc. Am.* 129 (6) (2011) 3544–3561.
- [16] C. Wei, K.K. Muraleetharan, A continuum theory of porous media saturated by multiple immiscible fluids: I. Linear poroelasticity, *Internat. J. Eng. Sci.* 40 (16) (2002) 1807–1833.
- [17] I. Tsimpanogiannis, Y. Yortsos, An effective continuum model for the gas evolution in internal steam drives, *SPE J.* 8 (3) (2003) 262–271.
- [18] A. Turgut, T. Yamamoto, Measurements of acoustic wave velocities and attenuation in marine sediments, *J. Acoust. Soc. Am.* 87 (6) (1990) 2376–2383.
- [19] W. Liu, Y. Li, B. Wang, Gas permeability of fractured sandstone/coal samples under variable confining pressure, *Transp. Porous Med.* 83 (2) (2010) 333–347.

- [20] D. Jones, M. Wilson, W. McHardy, Lichen weathering of rock-forming minerals: application of scanning electron microscopy and microprobe analysis, *J. Microsc.* 124 (1) (2011) 95–104.
- [21] L.M. Keller, L. Holzer, R. Wepf, P. Gasser, B. Münch, P. Marschall, On the application of focused ion beam nanotomography in characterizing the 3d pore space geometry of opalinus clay, *Phys. Chem. Earth* 36 (17) (2011) 1539–1544.
- [22] C. Appoloni, C.P. Fernandes, C.R.O. Rodrigues, X-ray microtomography study of a sandstone reservoir rock, *Nucl. Instrum. Methods A* 580 (1) (2007) 629–632.
- [23] D.A. Coker, S. Torquato, J.H. Dunsmuir, Morphology and physical properties of fontainebleau sandstone via a tomographic analysis, *J. Geophys. Res. Solid Earth* 101 (B8) (1996) 17497–17506.
- [24] P. Spanne, J.F. Thovert, C.J. Jacquin, W.B. Lindquist, K.W. Jones, P.M. Adler, Synchrotron computed microtomography of porous media: topology and transports, *Phys. Rev. Lett.* 73 (1994) 2001–2004.
- [25] C.L.Y. Yeong, S. Torquato, Reconstructing random media, *Phys. Rev. E* 57 (1998) 495–506.
- [26] H. Okabe, M.J. Blunt, Pore space reconstruction using multiple-point statistics, *J. Petrol. Sci. Eng.* 46 (1) (2005) 121–137.
- [27] S. Torquato, Statistical description of microstructures, *Ann. Rev. Mater. Sci.* 32 (1) (2002) 77–111.
- [28] P.E. Øren, S. Bakke, Process based reconstruction of sandstones and prediction of transport properties, *Transp. Porous Med.* 46 (2) (2002) 311–343.
- [29] M.J. Blunt, B. Bijeljic, H. Dong, O. Gharbi, S. Iglauer, P. Mostaghimi, A. Paluszny, C. Pentland, Pore-scale imaging and modelling, *Adv. Water Resour.* 51 (2013) 197–216.
- [30] F. Latief, B. Biswal, U. Fauzi, R. Hilfer, Continuum reconstruction of the pore scale microstructure for fontainebleau sandstone, *Physica A* 389 (8) (2010) 1607–1618.
- [31] F.J. Lucia, *Carbonate Reservoir Characterization*, Springer, 2007.
- [32] Y. Jiao, F. Stillinger, S. Torquato, Modeling heterogeneous materials via two-point correlation functions. ii. Algorithmic details and applications, *Phys. Rev. E* 77 (3) (2008) 031135.
- [33] N. Otsu, A threshold selection method from gray-level histograms, *Automatica* 11 (285–296) (1975) 23–27.
- [34] A. Kaestner, E. Lehmann, M. Stampanoni, Imaging and image processing in porous media research, *Adv. Water Resour.* 31 (9) (2008) 1174–1187.
- [35] P. Iassonov, T. Gebrenegus, M. Tuller, Segmentation of X-ray computed tomography images of porous materials: a crucial step for characterization and quantitative analysis of pore structures, *Water Resour. Res.* 45 (9) (2009) W09415.
- [36] M. Berthod, Z. Kato, S. Yu, J. Zerubia, Bayesian image classification using markov random fields, *Image Vis. Comput.* 14 (4) (1996) 285–295.
- [37] W. Lindquist, A. Venkatarangan, Investigating 3d geometry of porous media from high resolution images, *Phys. Chem. Earth PT A* 24 (7) (1999) 593–599.
- [38] G. Zack, W. Rogers, S. Latt, Automatic measurement of sister chromatid exchange frequency, *J. Histochemistry Cytochemistry* 25 (7) (1977) 741–753.
- [39] N.R. Pal, S.K. Pal, Entropic thresholding, *Signal Process.* 16 (2) (1989) 97–108.
- [40] C.E. Krohn, A.H. Thompson, Fractal sandstone pores: automated measurements using scanning-electron-microscope images, *Phys. Rev. B* 33 (1986) 6366–6374.
- [41] E. Schlüter, R. Zimmerman, P. Witherspoon, N. Cook, The fractal dimension of pores in sedimentary rocks and its influence on permeability, *Eng. Geol.* 48 (3) (1997) 199–215.
- [42] H. Xie, *Fractals in Rock Mechanics*, Vol. 1, Taylor & Francis, 1993.
- [43] A. Radlinski, E. Radlinska, M. Agamalian, G. Wignall, P. Lindner, O. Randl, Fractal geometry of rocks, *Phys. Rev. Lett.* 82 (1999) 3078–3081.
- [44] B. Yu, J. Li, Some fractal characters of porous media, *Fractals* 9 (03) (2001) 365–372.
- [45] R. Peng, H. Xie, Y. Ju, Computation method of fractal dimension for 2-d digital image, *J. China Univ. Mining Tech.* 33 (1) (2004) 19–24.
- [46] C.L.Y. Yeong, S. Torquato, Reconstructing random media. ii. Three-dimensional media from two-dimensional cuts, *Phys. Rev. E* 58 (1998) 224–233.
- [47] C. Manwart, S. Torquato, R. Hilfer, Stochastic reconstruction of sandstones, *Phys. Rev. E* 62 (1) (2000) 893.
- [48] S. Schlüter, H. Vogel, On the reconstruction of structural and functional properties in random heterogeneous media, *Adv. Water Resour.* 34 (2) (2011) 314–325.
- [49] D.A. Jerram, M.D. Higgins, 3d analysis of rock textures: quantifying igneous microstructures, *Elements* 3 (4) (2007) 239–245.
- [50] F. Meyer, Topographic distance and watershed lines, *Signal Process.* 38 (1) (1994) 113–125.
- [51] J.B. Roerdink, A. Meijster, The watershed transform: definitions, algorithms and parallelization strategies, *Fund. Inform.* 41 (1) (2000) 187–228.
- [52] H. Blum, A transformation for extracting new descriptors of shape, *Models Percep. Speech Visual Form* 19 (5) (1967) 362–380.
- [53] R. Al-Raoush, K. Thompson, C.S. Willson, Comparison of network generation techniques for unconsolidated porous media, *Soil Sci. Am. J.* 67 (6) (2003) 1687–1700.
- [54] A. Sheppard, R. Sok, H. Averdunk, Improved pore network extraction methods, in: *International Symposium of the Society of Core Analysts*, 2005, pp. 21–25.
- [55] M. Prodanović, W. Lindquist, R. Seright, 3d image-based characterization of fluid displacement in a berea core, *Adv. Water Resour.* 30 (2) (2007) 214–226.
- [56] S. Robinson, J. Jovicich, B0 mapping with multi-channel rf coils at high field, *Magn. Reson. Med.* 66 (4) (2011) 976–988.